3654–3662 *Nucleic Acids Research, 2017, Vol. 45, No. 7* *Published online 28 February 2017*
doi: 10.1093/nar/gkx148

Conformational polymorphism or structural invariance in DNA photoinduced lesions: implications for repair rates

François Dehez[1,2,3,*], Hugo Gattuso[1,2], Emmanuelle Bignon[4,5], Christophe Morell[4], Elise Dumont[5,*] and Antonio Monari[1,2,*]

[1]CNRS, Theory-Modeling-Simulation, SRSMC F-54506 Vandoeuvre-lès-Nancy, France, [2]Université de Lorraine, Theory-Modeling-Simulation, SRSMC F-54506 Vandoeuvre-lès-Nancy, France, [3]Laboratoire International Associé Centre National de la Recherche Scientifique et University of Illinois at Urbana Champaign, [4]Institut des Sciences Analytiques, UMR 5280, Université de Lyon1 (UCBL) CNRS, ENS Lyon, Lyon, France and [5]Université de Lyon, ENS de Lyon, CNRS, Université Lyon 1, Laboratoire de Chimie UMR 5182, F69342 Lyon, France

Received December 20, 2016; Revised February 06, 2017; Editorial Decision February 20, 2017; Accepted February 21, 2017

ABSTRACT

DNA photolesions constitute a particularly deleterious class of molecular defects responsible for the insurgence of a vast majority of skin malignant tumors. Dimerization of two adjacent thymines or cytosines mostly gives rise to cyclobutane pyrimidine dimers (CPD) and pyrimidine(6-4)pyrimidone 64-PP as the most common defects. We perform all-atom classical simulations, up to 2 μs, of CPD and 64-PP embedded in a 16-bp duplex, which reveal the constrasted behavior of the two lesions. In particular we evidence a very limited structural deformation induced by CPD while 64-PP is characterized by a complex structural polymorphism. Our simulations also allow to unify the contrasting experimental structural results obtained by nuclear magnetic resonance or Förster Resonant Energy Transfer method, showing that both low and high bent structures are indeed accessible. These contrasting behaviors can also explain repair resistance or the different replication obstruction, and hence the genotoxicity of these two photolesions.

INTRODUCTION

DNA is well renown for its photostability, (1–3) which is a key feature to ensure genome stability and avoid mutations or carcinogenesis (4,5). Nucleobases and nucleic acids absorb in the UV spectrum, mostly in the UVB and slightly in the UVA region due to excitonic coupling. In spite of the existence of efficient photophysical channels (6) allowing non-reactive relaxation, UV absorption opens photochemical pathways leading to nucleobase modification (7). The most common DNA damages produced upon direct UV absorption are characterized by the dimerization of two adjacent, π-stacked pyrimidine rings in B-DNA (see Figure 1) (8–10). Ultimately, photoinduced DNA lesions may induce harmful effects at the cellular level that, in the case of eukaryotic organisms, may be translated into mutation, skin aging and carcinogenesis (11). Indeed, UV absorption, and unprotected sun exposure, are nowadays recognized as the main causes of malignant skin tumors. From a molecular point of view, tumor insurgence is mostly associated with the presence of cyclobutane pyrimidine dimers (CPD) and/or pyrimidine(6-4)pyrimidone 64-PP (8), both lesions being mutagenic and possibly inducing genome instability with differential biological effects (12,13).

UVB irradiation of cells (245 nm) generates CPD as the most abundant photolesions while 64-PP, resulting from the excitation to higher lying electronic states (14), accounts for ∼20% of the defects formed (15,16). Processing efficiency is especially low for CPD (17), and in particular way less efficient than for 64-PP (15). For the repair of both lesions the nucleotide excision repair (NER) mechanism is mobilized (18). However, NER is known to participate in case of strongly distorted DNA structures and in the presence of bulky lesions. Hence, since deformation plays a fundamental role in the lesion recognition (19) a detailed understanding of the structural and dynamical signatures of photolesions is necessary to allow for a rationalization of repair rates (20–23).

X-ray or nuclear magnetic resonance (NMR) structures are indeed available for 6-4PP complexed with repair enzymes (photolyase (17)), that lead to the understanding

*To whom correspondence should be addressed. Tel: +33 372745278; Fax: +33 372745271; Email: antonio.monari@univ-lorraine.fr
Correspondence may also be addressed to François Dehez. Tel: +33 372745076; Fax: +33 372745271; Email: francois.dehez@univ-lorraine.fr
Correspondence may also be addressed to Elise Dumont. Tel: +33 472728846; Fax: +33 4 72728080; Email: elise.dumont@ens-lyon.fr

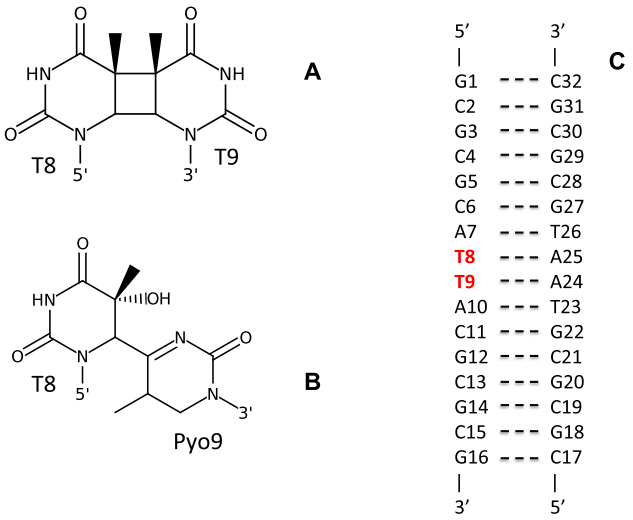

Figure 1. Molecular formula of CPD (**A**) and 64-PP (**B**). The 16 bp DNA double strand is also schematically reported with the bases' numbering (**C**). The two adjacent thymines at positions 8 and 9 (boldfaced in red) are the ones dimerizing to form the photolesions. In the case of 64-PP, the ninth nucleobase (T9) will be denoted Pyo9, being transformed into a pyrimidone unit.

of the enzymatic pathway toward repair at the molecular level (24), also thanks to molecular modeling and simulations (25,26). Yet structural resolution is far less often available for short oligonucleotides containing this photodamage. Two structures for solvated decamers containing 64-PP were reported (27–29), while most recently the structure of a 64-PP containing strand embedded within an histone (23) has been resolved. Other less direct measurements based on Förster resonant energy transfer (FRET) have also been published (30). Interestingly, the experimental determinations provided rather contrasting results: FRET measurements suggest a low DNA bending comparable to the one of the undamaged oligomers, as revealed by the large end-to-end distance of the strand, while X-ray and NMR agree on large bending going up to 44°. If the crystal packing or the interaction with histones can strongly modify the native structural properties of the DNA strands, still the experimental results in solution should be rationalized. Molecular dynamics (MD) simulations have been performed in the past on solvated oligonucleotides (31) or on oligonucleotides interacting with repair enzymes. (15,17,23). The pioneer simulation by Kollman's group (31) reported a very low bending for the 64-PP containing strand, however, the time-scales of the simulations were generally too small to capture their high structural flexibility. Also the structure of CPD containing oligomers has been resolved in the past concluding in favor of a general low bending of the DNA strand, (32) also in agreement with theoretical analysis (33). However, bending up to 30° have also been reported (34). While the repair mechanisms are now well understood owing to numerous and converging experimental (35) and modeling studies (36), insights are still scarce concerning the DNA-enzyme interaction leading to lesion recognition.

Structural deformation and strand flexibility have strong influence on the repair rates of DNA lesions. Indeed while bulky and important deformations are necessary to allow recognition by repair machinery (19), especially NER, flexibility has also been invoked as a factor enhancing the repair propensity of DNA lesions (37).

The use of well-calibrated (38,39), long-scale MD techniques allowing for an extended sampling of the conformational space of the DNA strand are needed to achieve a clear atomostic-scale characterization of the structural reorganization induced by photolesions. More importantly, sufficiently long MD will be able to capture the dynamical evolution of the structural deformation and hence will allow to properly assess the eventual polymorphisms exhibited by the damaged DNA oligonucleotides. MD simulations have been used to ultimately evidence the structural modification induced on DNA oligomers by oxidative lesions, intra- and inter-strand crosslinks, or via the interaction with exogenous and endogenous drugs (40–44). Recently, the structural deformations induced by clustered abasic sites have been correlated to the repair rate in human and bacterial organisms (21,22).

In this work we report an extensive all-atom MD simulation, up to the μs time scale, of DNA oligomers containing one CPD or one 64-PP damage, respectively; compared to the dynamics of the control undamaged B-DNA strand. The different structural behavior induced by the two lesions will be clearly assessed and compared to the evolution of the native B-DNA. The negligible deformations produced by CPD, and the extended polymorphism induced by 64-PP will be deeply analyzed and correlated with the low repair or the replication obstruction of the two photolesions.

MATERIALS AND METHODS

Computational protocol

For all the subsequent study we consider a 16-bp DNA strand (see Figure 1); the choice of a longer oligonucleotide instead of the 10-bp resolved by Lee *et al.*, has been done to avoid instability at the oligomer terminal bases. Starting from the same oligomer the lesion was produced by dimerization of the thymines at position 8 and 9, to obtain one CPD or a 64-PP, respectively. All atom MD simulations were performed with Amber16 (45) and NAMD (46) codes for the three systems, B-DNA, CPD and 64-PP. DNA nucleobases were represented by the parmbsc0 force field (47,48). The performance of the parmbsc0 force field has also been tested against the recently developed bsc1 (38) corrections and shown to perform analogously. In particular over the 150 ns dynamics we observed similar transitions between conformers as the ones described with parmbsc0 force field. The parameters for the CPD and 64-PP lesion were assigned according to the standard RESP protocol (49). We note that they are in very good agreement with the ones derived by Kollman *et al.* (31). Water molecules were represented by TIP3P model and 30 potassium cations were added to the simulation box to assure neutrality. A detailed description of the computational protocol and the force-field parameters for the damaged base can be found in Supplementary Data. After thermalization and equilibration production MD has been performed in the constant pressure and temperature (NPT) ensemble (300 K, 1 atm). In the case of 64-PP a 2 μs trajectory has been performed in order to properly

explore the conformational space evidencing the dynamical equilibrium between different conformers. In order to characterize the global DNA behavior the DNA bending angle was calculated along the three trajectories with Curves+ (50). The compactness of the structures was assessed by the calculation of the solvent accessible surface area (SASA) (51) obtained post-processing the MD trajectories with the measure command of VMD (52) and a probe radius of 1.4 Å. The local deformation was further explored by analyzing the extent of π-stacking between the nucleobases adjacent to the lesion as obtained by the distance between the aromatic rings.

RESULTS

In a first step we assess the structural distortion of the 16-bp duplex containing a photolesion through two global parameters namely the DNA helical bending, and the SASA. Helical bending in particular also allows for a straightforward comparison with experimental results. In Figure 2, we report the distributions of the bending angle as calculated by Curves+ (50) in the case of the native B-DNA and in presence of CPD or 64-PP. CPD bending distribution almost perfectly overlaps the one of the control double-stranded sequence, with maximum values at around 20° and 18°, respectively. Instead, the situation is stunningly different for 64-PP (Figure 2C), where the bending is much more dispersed. Indeed, one can evidence two peaks: a first one centered at around 20°, overlapping with the control B-DNA sequence and the CPD containing duplex, and a second one appearing at larger values (40°). We also point the presence of a less populated yet clear shoulder at even higher bending angles.

SASA values, presented in Figure 2 rightside, globally show similar tendencies as for the bending and clearly points in favor of marked deformations only in the case of 64-PP. Once again CPD and B-DNA distributions almost perfectly overlaps both in terms of the maximum value and of the band shape. On the other hand, three maxima, two well resolved peaks and a shoulder, can be evidenced for 64-PP. The solvent accessibility values indicate that 64-PP spans an ensemble of conformations, some of them being quite compact (low SASA) and other presenting a large surface area (high SASA).

In Figure 3 these tendencies are exemplified by the comparison of the representative structures of B-DNA and CPD containing oligomers (that indeed appears indistinguishable), with two highly distorted 64-PP conformations characterized by a low and high bending, and by different compactness due to the formation of hollow structures.

In order to assess the convergence of 64-PP simulation we also performed parallel tempered replica exchange (53) representing a total sampling time of about 5 μs. The distribution of bending and SASA obtained for 64-PP are reported in Figure 4. Globally the enhanced sampling procedure confirms the previous results and in particular the polymorphism exhibited by 64-PP containing strand, in particular both high and low bending values are once again represented. The SASA distribution is also extremely broad and point toward the coexistence of different structures exhibiting different compactness, however the peak for low SASA, i.e. compact structure, is much less well resolved, indicating a lower population of the corresponding conformers. Indeed, the relative population of the different structures appears difficult to reproduce and would necessitate a prohibitively computational effort, nonetheless the global consideration over the dynamic equilibrium leading to polymorphism still holds.

Hence, a first stunning difference between CPD and 64-PP can be unequivocally invoked, i.e. the structural invariance of the former compared to the important deformation, and the flexibility, induced by the latter. As indicated by the global descriptors 64-PP exhibits polymorphism and thus deserves a closer attention to clearly identify the complex behavior induced by this lesion. Figure 5 provides the time evolution of the distance between the nucleobases in the vicinity of the 64-PP lesion (see Supplementary Data for a proper definition). This parameter has been chosen since it allows to quantify the extent of the formation of π-stacking interactions. Along the 2 μs of the trajectory 64-PP explores a rather large conformational space with a complex equilibrium between different conformations, characterized by different π-stacking interaction patterns between the nucleobases. Quite importantly, the equilibrium is extremely dynamic, the stable conformations are separated by some transition regions, and the conformers can have multiple occurrences during the time series. In partial contrast to the global parameters (bending and SASA) the use of a more local descriptor clearly indicates the presence of at least five distinct conformations. However, the use of unconstrained MD does not allow to estimate the absolute population rates between the conformers nor to *a priori* exclude the existence of other possible stable structures.

Figure 6 provides representative snapshots of all the five stable equilibrium conformations together with schematic diagrams depicting the interactions taking place and stabilizing the specific conformations. It is important to stress out the considerable structural differences as well as the high variability of the coupling between the different nucleobases. Hence, one can safely conclude that 64-PP does not present a well-defined unique structure but rather a complex equilibrium between different conformations whose structure and properties strongly differ. Once again the same behavior is confirmed by the analysis of the distances distribution for the unbiased and parallel tempering simulation as reported in Supplementary Data, even though, as already evidenced for the SASA the relative population is slightly altered.

We seek to identify the rather complex reorganization pattern induced by 64-PP and the non-covalent interactions that come into play to stabilize the duplex after the induction of the covalent-linkage. Cartoon representations are given in Figure 6, together with schemes depicting the spatial arrangement of the nucleobases: hereafter the thymine at position 9 will be indicated as Pyo9 since it is the one forming the pyrimidone moiety (Figure 1). Indeed, the large conformational landscape explored at the μs range arises from the fact the duplex can rearrange to favor interstrand dispersive interactions (green boxes in Figure 6) and hydrogen bonding with offset nucleobases (dashed blue line), which in some cases can lead to the exclusion of vicinal nuclebases.

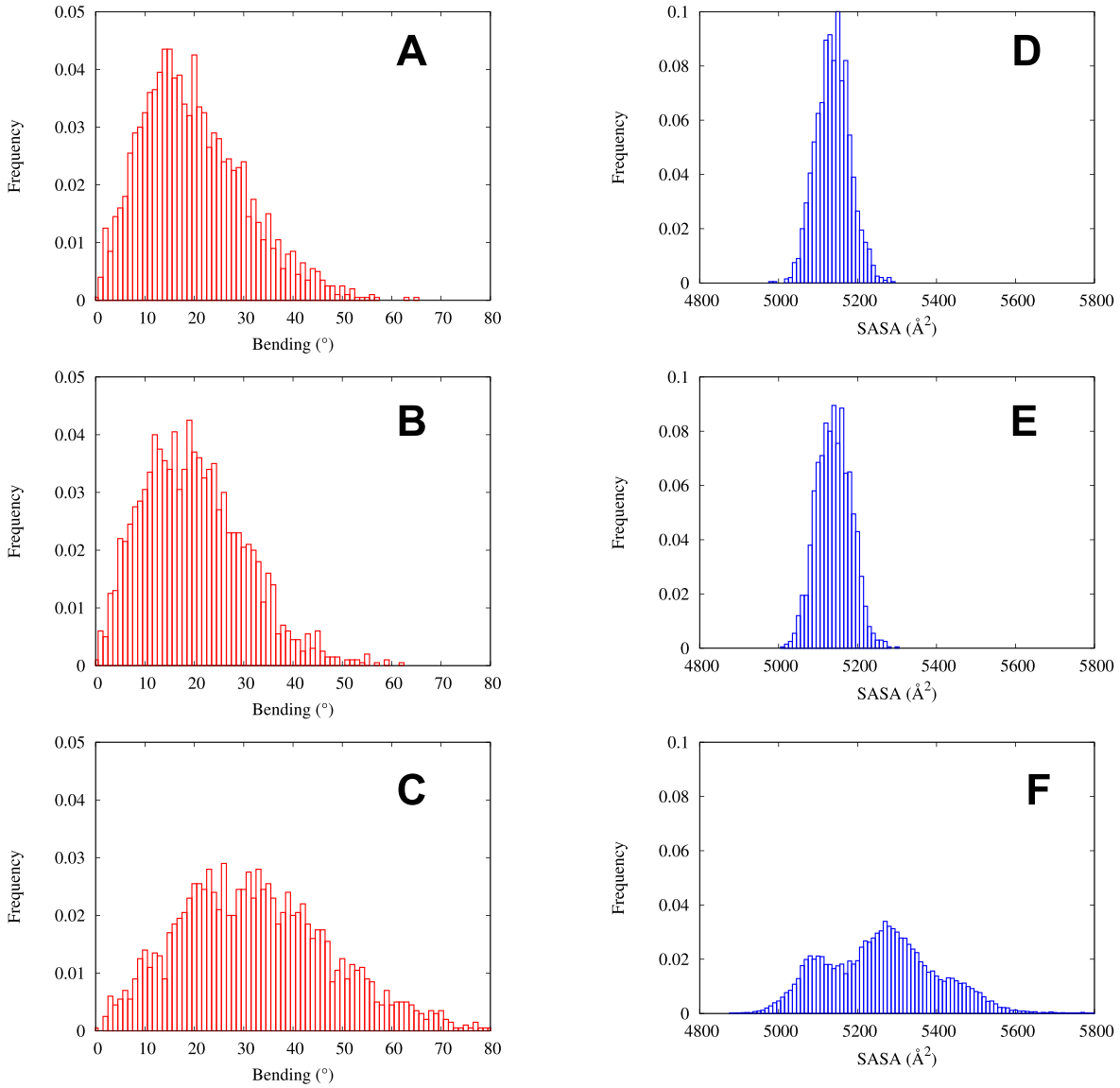

Figure 2. Distribution of the total DNA bending (in red) for B-DNA (**A**), CPD (**B**) and 64-PP (**C**); and of the SASA (in blue) for B-DNA (**D**), CPD (**E**) and 64-PP (**F**).

Conf-(1) maintains a spatial proximity between the damaged T8 and the originally complementary adenine A24, at a distance of ∼4Å which actually corresponds to the π-stacking. A24 can indeed no longer be Watson–Crick paired with Pyo9 and instead the helix readapts by a local shrinkage to afford a stacking between Pyo9 and A24, the latter behaving as an orphan nucleobasis.

The duplex then evolves toward Conf-(2) which is stabilized by conserving an extended stacking on the 64-PP complementary strand involving thymines and adenines (from T23 up to T26) while interstrand dispersive interactions are no more present. Interestingly, this conformation corresponds to a maximal curvature, as verified by the bend angle (54.3°).

After 1 μs, the duplex rearranges to adopt a more straight and compact conformation Conf-(3) with interstrand π-stacking between Pyo9 and T26, but also between A7 and A25. These interactions narrows the B-helix and contributes to decrease the bend (26.7°), whereas no new hydrogen bonds comes into play to stabilize the damaged duplex.

At around 1.8 μs a conformation rather similar to Conf-(2), that we will call Conf-(4), is found to be characterized by a proximity between the damaged Pyo9 and T26. Also this conformation presents an extended stacking on the lesion's complementary strand going from T23 to T26 and a high bending (49.6°). However, differently from Conf-(2), the stacking region is shifted downward.

Oppositely, Conf-(5) is the first structure exhibiting a gap between A24 and A25, which lies at about 7 Å, while T8 gets close to the A7–T26 base pair still locked in the Watson–Crick pairing. Ultimately, the alcohol function of T8 interacts with the oxygen O2 of T26 to form a stable hydrogen-

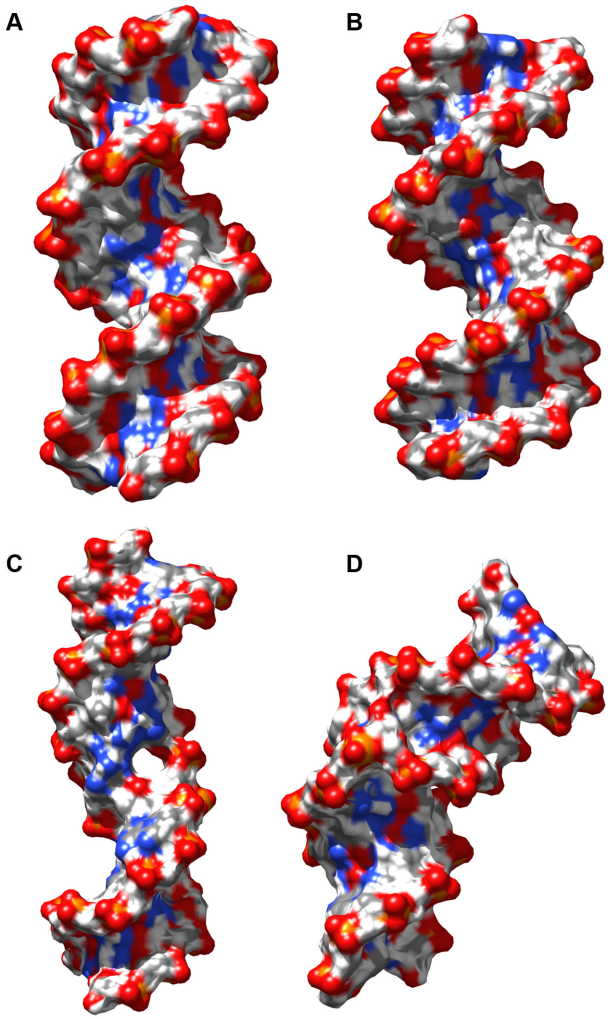

Figure 3. Representative snapshots rendered in surface mode for B-DNA (**A**), CPD (**B**) and 64-(PP) in a low bending high SASA conformation (**C**) and in a high bending low SASA one (**D**).

bond. Conf-(5) duplex presents a globally low bending just slightly higher than the average value for the control B-DNA sequence.

The tendency of A24 to seek opportunistic interactions to compensate for the lack of pairing with the complementary thymine is a constant all along our dynamics. The same behavior is also experienced by Pyo9 that in particular seeks to adopt conformations allowing dispersive interactions with A25. The coupled perturbation of the arrangements of the two strands propagates up to A10 and G22 which may develop non-conventional π-stackings interaction, while the Watson Crick pairing with T23 and C11 is maintained. Conf-(2) and Conf-(4) are both characterized by large bend angles of $\sim 50^{\circ}$, yet they differ markedly by the local structural rearrangement. Indeed, Conf-(4) is pushing A7 to an extrahelical position allowing to maintain C6...G23 and A10...T23 pairings. Note also that, Conf-(4) and Conf-(5) clearly exhibit a hole structure in correspondence of the lesions, leading to high values of SASA; the same behavior, even if less pronounced, is also be evidenced for Conf-(2). Correspondingly, the complex nucleobase rearrangement, necessary to accommodate the intrastrand cross-links created between Pyo9 and T8 leads to marked variations of the total bend angle. However, in all the cases, bulges and helical distortion in the region corresponding to the lesions are clearly identified. The existence of rather large structural deformations and a large reorganization of the helical parameters, in particular in the vicinity of the lesion, are also confirmed by the time-series and the distribution of some relevant DNA structural parameters extracted with Curves+ (50), such as the minor and major groove width and depth (see Supplementary Data). Indeed the base-pairs surrounding the lesions (from 7 to 10) appears as the most influenced and exhibit a strong variation correlating well with the distribution of the distances previously analyzed. Most notably, one can observe a general shrinking of the major groove especially evident for Conf-(2) and Conf-(3) while Conf-(1), Conf-(4), and especially Conf-(5) are characterized by a slight enlargement of the major groove width. Minor groove, on the contrary, appears less influenced and correlation extracted from this parameters less straightforward, even though the value of the groove depth in the correspondence of the lesion peaks to zero indicating an important shrinking of the strand.

DISCUSSION AND CONCLUSIONS

The behavior of the two most common DNA photoproducts, CPD and 64-PP, has been fully characterized by long timescale, all-atom simulations. In particular, it has been clearly evidenced that CPD induces a minimal structural deformation. The CPD containing duplex is indeed absolutely comparable to the native B-DNA, both in terms of bending and SASA distribution. In addition, only one stable conformation is observed and all the local and global structural parameters are much similar to the ones of the undamaged strand. CPD is one of the only lesions in B-DNA implying the formation of two covalent bonds tethering the adjacent thymines: rather logically, this confers more rigidity and locks the structure, decreasing the rotational freedom.

On the other hand, the situation is totally reversed in the case of 64-PP. Indeed, 64-PP is characterized by a dramatic structural deformation centered around the lesion and propagating to a large part of the duplex. At least three maxima can be evidenced in the distributions of both SASA and bending angle, pointing toward the coexistence of compact and surface exposed structures, as well as bent and straight arrangements.

Our simulations unify the complex and somewhat conflicting panorama of experimentally-based 64-PP, and CPD structural resolution. Indeed, while the general CPD low bending is recovered, as shown by the most probable angle, the distribution width clearly indicates that values close to 30° cannot be ruled out and can occur at room temperate. On the other hand, in the case of 64-PP our results show that both NMR (29) and FRET (30), i.e. high and low bending, are possible due to its polymorphisms and depending on the specific conformations. Indeed, we also report in Supplementary Data the distribution of the end-to-end distance of the DNA double strand we observe the presence of two peaks at distance of 55 or 60 Å that correlates well with the

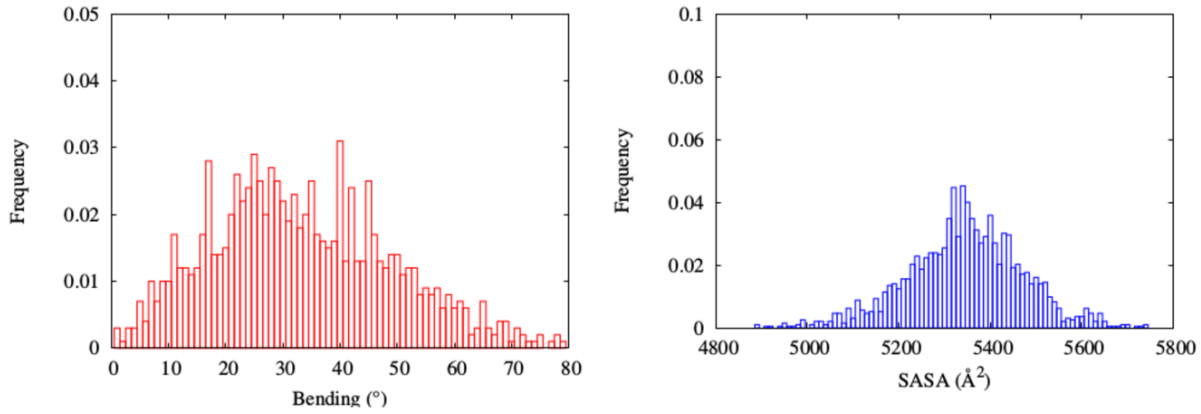

Figure 4. Distribution of the total DNA bending (red) and SASA (blue) obtained from replica exchange parallel tempering.

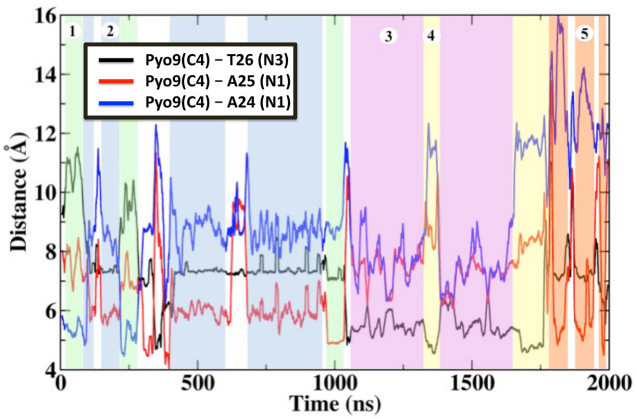

Figure 5. Time evolution of internucleobases distances measured between Pyo9 and A24, A25 and T26, characterizing the different π-stacking formations and hence the increased flexibility and polymorphism upon formation of 64-PP. The regions corresponding to different conformations are indicated by colored background.

values reported in (30) for strands having the same number of base pairs. The NMR predicted bending value of around 40° corresponds to one of the maximum of the bending distribution, on the other hand the FRET results are consistent with the second maximum appearing at lower angle and leading to bending comparable to the ones of native B-DNA.

Recently DNA polymorphism also in the case of non-damaged strands has been proved for instance by circular dichroism techniques (54) or by molecular simulation (55), it has also been correlated to the insurgence of different pathologies in particular when involving gene regulatory areas such as CpG islands (56) or telomeres (57,58).

As it is clearly shown by our simulations, 64-PP is actually experiencing structural polymorphism that ends up in a dynamic equilibrium between different conformations whose local structural parameters differ significantly. Such polymorphism is definitively striking also when compared to the more predictable structural rearrangements produced by oxidatively-induced intrastrand cross-link lesions (41,59). The former lesions rearrange to restore B-helicity and as a consequence they lead to less extreme bending values and a globally more rigid structure.

The observed contrasting structural behavior may indeed be correlated to the repair and replication rate of the two lesions, and hence their toxicity. Indeed, CPD extremely low repair rate may be seen as a direct consequence of the absence of relevant structural modifications compared to B-DNA. This fact indeed, hampers the lesion's recognition since a common recognition pattern is the structural deformation induced by the damage (37). In a simplified way, one may say that CPD actually masks itself and hides between the undamaged B-DNA, hence escaping recognition and repair. However, its rigidity also constitutes a blockage to the replication process that ultimately results in the limited mutagenic power especially as compared to 64-PP (60).

64-PP on the other hand adopts a totally different strategy, the large structural deformation experienced by this lesion is indeed consistent with the mobilization of the NER repair machinery and the lesions is processed much more efficiently than CPD (61). However, due to the observed polymorphism no single stable structure can be evidenced, and the lesion is constantly shifting back and forth between different conformations, and as a consequence the recognition by enzymes can be made more difficult. This is particular true since some of the conformers present very different local deformations and interaction patterns, as well as different global parameters such as bending and surface accessibility. Furthermore, the flexibility and polymorphisms of 64-PP also correlates with the absence of unyielding obstruction to the DNA replication process (62) leading to the accumulation of mutations at the photolesion spot. Indeed, the easy replication of 64-PP damaged strand is recognized as one of the reason of 64-PP high toxicity and mutagenicity (63), and the observed polymorphism and the different nucleobase interaction patterns may also explain the large spectrum of observed mutations.

It is however important to underline that we may anticipate a different behavior of 64-PP when complexed with histones in a nucleosomal environment, as surmised by Akihisa *et al.* (23). In particular the constraints due to interacting proteins and the compact nucleosomal environment may restrict the accessibility of the explored conformational

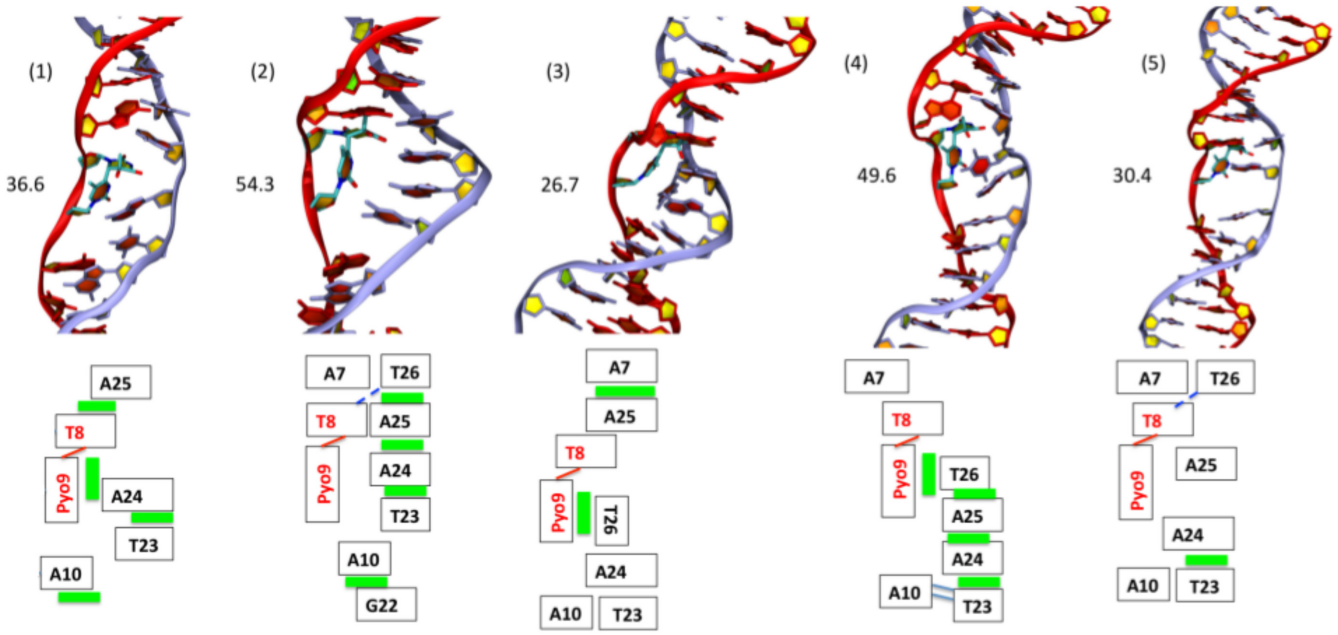

Figure 6. Cartoon representations of five representative conformation observed along the 2 μs trajectory. The schematic depiction of the interaction patterns is given in the bottom figures for each conformer, where green boxes represent π-stacking and blue lines hydrogen bonds. The value of the bending angle for each conformer is indicated in parenthesis.

landscape, still the influence of flexibility on the replication obstruction will hold.

Our simulations have allowed to shed a new light on the complex and dynamic structure of two very important lesions exploring complex free energy surfaces. They sketched two different and opposed behaviors: structural invariance (CPD) or conformational polymorphism (64-PP). In the following, and in order to draw a more precise correlation with repair efficiency, we preview to extend this study to the interaction between the different lesions' conformers and both nucleosomal environment and the repair enzymes.

SUPPLEMENTARY DATA

Supplementary Data are available at NAR Online.

ACKNOWLEDGEMENTS

Supports from the University of Lorraine and ENS Lyon is gratefully acknowledged. AM thanks CNRS for support under the project 'Action pour l'interdisciplinarite 2016'. Support from the French Grand-Est region under the Idea project is acknowledged too. This work was performed within the framework of the LABEX PRIMES (ANR-11-LABX-0063) of Université de Lyon, within the program 'Investissements d'Avenir' (ANR-11-IDEX-0007) operated by the French National Research Agency (ANR).

FUNDING

University of Lorraine; ENS Lyon; CNRS under the project 'Action pour l'interdisciplinarite 2016' (to A.M.); French Grand-Est region under the Idea project; LABEX PRIMES of Université de Lyon [ANR-11-LABX-0063]; French National Research Agency (ANR) 'Investissements d'Avenir' program [ANR-11-IDEX-0007]. Funding for open access charge: University of Lorraine and Lyon.
Conflict of interest statement. None declared.

REFERENCES

1. Satzger,H., Townsend,D., Zgierski,M.Z., Patchkovskii,S., Ullrich,S. and Stolow,A. (2006) Primary processes underlying the photostability of isolated DNA bases: Adenine. *Proc. Natl. Acad. Sci. U.S.A.*, **103**, 10196–10201.
2. Barbatti,M., Aquino,A. J.A., Szymczak,J.J., Nachtigallova,D., Hozba,P. and Lischka,H. (2014) Relaxation mechanisms of UV-photoexcited DNA and RNA nucleobases. *Proc. Natl. Acad. Sci. U.S.A.*, **107**, 21453–21458.
3. Buchner,F., Nakayama,A., Yamazaki,S., Ritze,H.-H. and Loebcke,A. (2015) Excited-state relaxation of hydrated thymine and thymidine measured by liquid-jet photoelectron spectroscopy: experiment and simulation. *J. Am. Chem. Soc.*, **137**, 2931–2938.
4. Deman,J. and Van Larebeke,N. (2001) Carcinogenesis: mutations and mutagens. *Tumor Biol.*, 191–202.
5. Morley,A.A. and Turner,D.R. (1999) The contribution of exogenous and endogenous mutagens to in vivo mutations. *Mutat. Res.*, **428**, 11–15.
6. Gustavsson,T., Improta,R. and Markovitsi,D. (2010) DNA/RNA: building blocks of life under UV irradiation. *J. Phys. Chem. Lett.*, **1**, 2025–2030.
7. Cadet,J., Mouret,S., Ravanat,J.-L. and Douki,T. (2012) Photoinduced damage to cellular DNA: direct and photosensitized reactions'. *Photochem. Photobiol.*, **88**, 1048–1065.
8. Mitchell,D.L. and Nairn,R.S. (1989) The biology of the (6-4) photoproduct. *Photochem. Photobiol.*, **49**, 805–819.
9. Gonzalez-Ramirez,I., Roca-Sanjuán,D., Climent,T., Serrano-Perez,J.J., Merchan,M. and Serrano-Andres,L. (2011) On the photoproduction of DNA/RNA cyclobutane pyrimidine dimers. *Theor. Chem. Acc.*, **128**, 705–711.
10. Rauer,C., Nogueira,J.J., Marquetand,P. and Gonzalez,L. (2016) Cyclobutane thymine photodimerization mechanism revealed by nonadiabatic molecular dynamics. *J. Am. Chem. Soc.*, **138**, 15911–15916.

11. D'Orazio,J., Jarrett,S., Amaro-Ortiz,A. and Scott,T. (2013) UV radiation and the skin. *Int. J. Mol. Sci.*, **14**, 12222–12248.
12. Lo,H.-L., Nakajima,S., Ma,L., Walter,B., Yasui,A., Ethell,D.W. and Owen,L.B. (2005) Differential biologic effects of CPD and 6-4PP UV-induced DNA damage on the induction of apoptosis and cell-cycle arrest. *BMC Cancer*, **5**, 135.
13. Pfeifer,G.P. and Besaratinia,A. (2012) UV wavelength-dependent DNA damage and human non-melanoma and melanoma skin cancer. *Photochem. Photobiol. Sci.*, **11**, 90–97.
14. Banyasz,A., Douki,T., Improta,R., Gustavsson,T., Onidas,D., Vayá,I., Perron,M. and Markovitsi,D. (2012) Electronic excited states responsible for dimer formation upon UV absorption directly by thymine strands: joint experimental and theoretical study. *J. Am. Chem. Soc.*, **134**, 14834–14845.
15. Balajee,A.S., May,A. and Bohr,V.A. (1999) DNA repair of pyrimidine dimers and 6-4 photoproducts in the ribosomal DNA. *Nucleic Acids Res.*, **27**, 2511–2520.
16. Perdiz,D., Grof,P., Mezzina,M., Nikaido,O., Moustacchi,E. and Sage,E. (2000) Distribution and repair of bipyrimidine photoproducts in solar UV-irradiated mammalian cells: possible role of dewar photoproducts in solar mutagenesis. *J. Biol. Chem.*, **275**, 26732–26742.
17. Li,J., Liu,Z., Tan,C., Guo,X., Wang,L., Sancar,A. and Zhong,D. (2010) Dynamics and mechanism of repair of ultraviolet-induced (6-4) photoproduct by photolyase. *Nature*, **466**, 887–890.
18. Marteijn,J.A., Lans,H., Vermeulen,W. and Hoeijmakers,J. H.J. (2014) Understanding nucleotide excision repair and its roles in cancer and ageing. *Nat. Rev. Mol. Biol.*, **15**, 465–481.
19. Scharer,D.O. (2013) Nucleotide excision repair in eukaryotes. *Cold Spring Harb. Perspect. Biol.*, **5**, a012609.
20. Han,C., Srivastava,A.K., Cui,T., Wang,Q.-E. and Wani,A.A. (2016) Differential DNA lesion formation and repair in heterochromatin and euchromatin. *Carcinogenesis*, **37**, 129–138.
21. Bignon,E., Gattuso,H., Morell,C., Dehez,F., Georgakilas,A.G., Monari,A. and Dumont,E. (2016) Correlation of bistranded clustered abasic DNA lesion processing with structural and dynamic DNA helix distortion. *Nucleic Acids Res.*, **44**, 8588–8599.
22. Gattuso,H., Durand,E., Bignon,E., Morell,C., Georgakilas,A.G., Dumont,E., Chipot,C., Dehez,F. and Monari,A. (2016) Repair rate of clustered abasic DNA lesions by human endonuclease: molecular bases of sequence specificity. *J. Phys. Chem. Lett.*, **7**, 3760–3765.
23. Akihisa,O., Hiroaki,T., Wataru,K., Naoki,H., Syota,M., Mayu,H., Naoyuki,M., Tatsuya,T., Junpei,Y., Fumio,H. *et al.* (2015) Structural basis of pyrimidine-pyrimidone (64) photoproduct recognition by UV-DDB in the nucleosome. *Sci. Rep.*, **5**, 16330–16330.
24. Yamamoto,J., Martin,R., Iwai,S., Plaza,P. and Brettel,K. (2013) Repair of the (64) photoproduct by DNA photolyase requires two photons. *Angew. Chem. Int. Ed.*, **52**, 7432–7436.
25. Dokainish,H.M. and Kitao,A. (2016) Computational assignment of the histidine protonation state in (6-4) photolyase enzyme and its effect on the protonation step. *ACS Catal.*, **6**, 5500–5507.
26. Knips,A. and Zacharias,M. (2017) μABC: a systematic microsecond molecular dynamics study of tetranucleotide sequence effects in B-DNA. *Sci. Rep.*, **7**, 41324.
27. Kim,J.-K., Patel,D. and Choi,B.-S. (1995) Contrasting structural impacts induced by cis-syn cyclobutane dimers and (6-4) adduct in DNA duplex decamers: Implication in mutagenesis and repair activity. *Photochem. Photobiol.*, **62**, 44–50.
28. Kim,J.-K. and Choi,B.-S. (1995) The solution structure of DNA duplex-decamer containing the (6-4) photoproduct of Thymidylyl(3′–>5′)Thymidine by NMR and relaxation matrix refinement. *Euro. J. Biochem.*, **228**, 849–854.
29. Lee,J.-H., Hwang,G.-S. and Choi,B.-S. (1999) Solution structure of a DNA decamer duplex containing the stable 3′ T.G base pair of the pyrimidine(64)pyrimidone photoproduct [(64) adduct]: Implications for the highly specific 3′ T –> C transition of the (64) adduct. *Proc. Natl. Acad. Sci. U.S.A.*, **96**, 6632–6636.
30. Mizukoshi,T., Kodama,T.S., Fujiwara,Y., Furuno,T., Nakanishi,M. and Iwai,S. (2001) Structural study of DNA duplexes containing the (64) photoproduct by fluorescence resonance energy transfer. *Nucleic Acids Res.*, **29**, 4948–4954.
31. Spector,T.I., Cheatham,T.E. and Kollman,P.A. (1997) Unrestrained molecular dynamics of photodamaged DNA in aqueous solution. *J. Am. Chem. Soc.*, **119**, 7095–7104.
32. Wang,C.I. and Taylor,J.S. (1991) Site-specific effect of thymine dimer formation on dAn.dTn tract bending and its biological implications. *Proc. Natl. Acad. Sci. U.S.A.*, **88**, 9072–9076.
33. Cooney,M.G. and Miller,J.H. (1997) Calculated distortions of duplex DNA by a Cis, Syn cyclobutane thymine dimer are unaffected by a 3′ TpA step. *Nucleic Acids Res.*, **25**, 1432–1436.
34. Park,H., Zhang,K., Ren,Y., Nadji,S., Sinha,N., Taylor,J.-S. and Kang,C. (2002) Crystal structure of a DNA decamer containing a cis-syn thymine dimer. *Proc. Natl. Acad. Sci. U.S.A.*, **99**, 15965–15970.
35. Ando,H., Fingerhut,B.P., Dorfman,K.E., Biggs,J.D. and Mukamel,S. (2014) Femtosecond stimulated raman spectroscopy of the cyclobutane thymine dimer repair mechanism: a computational study. *J. Am. Chem. Soc.*, **136**, 14801–14810.
36. Masson,F., Laino,T., Tavernelli,I., Rothlisberger,U. and Hutter,J. (2008) Computational study of thymine dimer radical anion splitting in the self-repair process of duplex DNA. *J. Am. Chem. Soc.*, **130**, 3443–3450.
37. Yang,W. (2011) Surviving the Sun: repair and bypass of DNA UV lesions. *Protein Sci.*, **20**, 1781–1789.
38. Ivani,I., Dans,P.D., Noy,A., Perez,A., Faustino,I., Hospital,A., Walther,J., Andrio,P., Goni,R., Balaceanu,A. *et al.* (2016) Parmbsc1: a refined force field for DNA simulations. *Nat. Methods*, **38**, 55–58.
39. Perez,A., Luque,F.J. and Orozco,M. (2012) Frontiers in molecular dynamics simulations of DNA. *Acc. Chem. Res.*, **45**, 196–205.
40. Dumont,E. and Monari,A. (2015) Understanding DNA under oxidative stress and sensitization: the role of molecular modeling. *Front. Chem.*, **3**, 43.
41. Dumont,E., Drsata,T., Fonseca Guerra,C. and Lankas,F. (2015) Insights into the structure of intrastrand cross-link DNA lesion-containing oligonucleotides: G[85m]T and G[85]C from molecular dynamics simulations. *Biochemistry*, **54**, 1259–1267.
42. Dumont,E. and Monari,A. (2013) Benzophenone and DNA: Evidence for a double insertion mode and its spectral signature. *J. Phys. Chem. Lett.*, **4**, 4119–4124.
43. Nogueira,J.J. and Gonzalez,L. (2014) Molecular dynamics simulations of binding modes between methylene blue and DNA with alternating GC and AT sequences. *Biochemistry*, **53**, 2391–2412.
44. Spiegel,K., Rothlisberger,U. and Carloni,P. (2004) Cisplatin binding to DNA oligomers from hybrid car-parrinello/molecular dynamics simulations. *J. Phys. Chem. B*, **108**, 2699–2707.
45. Case,D., Betz,R., Botello-Smith,W., Cerutti,D., III,T.C., Darden,T., Duke,R., Giese,T., Gohlke,H., Goetz,A. *et al.* (2016) *AMBER 16*, University of California, San Francisco, CA.
46. Phillips,J.C., Braun,R., Wang,W., Gumbart,J., Tajkhorshid,E., Villa,E., Chipot,C., Skeel,R.D., Kale,L. and Schulten,K. (2005) Scalable molecular dynamics with NAMD. *J. Comput. Chem.*, **26**, 1781–1802.
47. Cornell,W.D., Cieplak,P., Bayly,C.I., Gould,I.R., Merz,K.M., Ferguson,D.M., Spellmeyer,D.C., Fox,T., Caldwell,J.W. and Kollman,P.A. (1995) A second generation force field for the simulation of proteins, nucleic acids, and organic molecules. *J. Am. Chem. Soc.*, **117**, 5179–5197.
48. Perez,A., Marchan,I., Svozil,D., Sponer,J., III,T.E.C., Laughton,C.A. and Orozco,M.2007 Refinement of the AMBER force field for nucleic acids: improving the description of alpha/gamma Conformers. *Biophysical.*, **92**, 3817–3829.
49. Wang,J., Wolf,R.M., Caldwell,J.W., Kollman,P.A. and Case,D.A. (2004) Development and testing of a general amber force field. *J. Comput. Chem.*, **25**, 1157–1174.
50. Lavery,R., Moakher,M., Maddocks,J.H., Petkeviciute,D. and Zakrzewska,K. (2009) Conformational analysis of nucleic acids revisited: Curves+. *Nucleic Acids Res.*, **37**, 5917–5929.
51. Shrake,A. and Rupley,J.A. (1973) Environment and exposure to solvent of protein atoms. Lysozyme and insulin. *J. Mol. Biol.*, **79**, 351–371.
52. Humphrey,W., Dalke,A. and Schulten,K. (1996) VMD—visual molecular dynamics. *J. Mol. Graph.*, **14**, 33–38.
53. Sugita,Y. and Okamoto,Y. (1999) Replica-exchange molecular dynamics method for protein folding. *Chem. Phys. Lett.*, **314**, 141–151.
54. Kypr,J., Kejnovska,I., Renciuk,D. and Vorlickova,M. (2009) Circular dichroism and conformational polymorphism of DNA. *Nucleic Acids Res.*, **37**, 1713–1725.

55. Pasi,M., Maddocks,J.H., Beveridge,D., Bishop,T.C., Case,D.A., Cheatham,T. III, Dans,P.D., Jayaram,B., Lankas,F., Laughton,C. *et al.* (2014) μABC: a systematic microsecond molecular dynamics study of tetranucleotide sequence effects in B-DNA. *Nucleic Acids Res.*, **42**, 12272–12283.
56. Dans,P.D., Faustino,I., Battistini,F., Zakrzewska,K., Lavery,R. and Orozco,M. (2014) Unraveling the sequence-dependent polymorphic behavior of d(CpG) steps in B-DNA. *Nucleic Acids Res.*, **42**, 11304–11320.
57. Cogoi,S., Paramasivam,M., Spolaore,B. and Xodo,L.E. (2008) Structural polymorphism within a regulatory element of the human KRAS promoter: formation of G4-DNA recognized by nuclear proteins. *Nucleic Acids Res.*, **36**, 3765–3780.
58. Gaynutdinov,T.I., Neumann,R.D. and Panyutin,I.G. (2008) Structural polymorphism of intramolecular quadruplex of human telomeric DNA: effect of cations, quadruplex-binding drugs and flanking sequences. *Nucleic Acids Res.*, **36**, 4079–4087.
59. Churchill,C.D., Eriksson,L.A. and Wetmore,S.D. (2016) DNA distortion caused by uracil-containing intrastrand cross-links. *J Phys. Chem. B*, **25**, 1195–1204.
60. Sale,J.E., Lehmann,A.R. and Woodgate,R. (2012) Y-family DNA polymerases and their role in tolerance of cellular DNA damage. *Nat. Rev. Mol. Cell Biol.*, **13**, 141–152.
61. Courdavaultas,S., Baudouinb,C., Charveronb,M., Canguilhemb,B., Faviera,A., Cadeta,J. and Douki,T. (2005) Repair of the three main types of bipyrimidine DNA photoproducts in human keratinocytes exposed to UVB and UVA radiations. *DNA Repair*, **4**, 836–844.
62. Kuang,Y., Sun,H., Blain,J.C. and Peng,X. (2012) Hypoxia-selective DNA interstrand cross-link formation by two modified nucleosides. *Chemistry*, **18**, 12609–12613.
63. Gentil,A., Page,F.L., Margot,A., Lawrence,C.W., Borden,A. and Sarasin,A. (1996) Mutagenicity of a unique thymine-thymine dimer or thymine-thymine pyrimidine pyrimidone (64) photoproduct in mammalian cells. *Nucleic Acids Res.*, **24**, 1837–1840.